



PERGAMON

Deep-Sea Research II 50 (2003) 141–166

DEEP-SEA RESEARCH
PART II

www.elsevier.com/locate/dsr2

Early evolution of an Agulhas Ring

C. Schmid^{a,*}, O. Boebel^b, W. Zenk^c, J.R.E. Lutjeharms^d, S.L. Garzoli^e,
P.L. Richardson^f, C. Barron^g

^aNOAA/AOML/PHOD, 4301 Rickenbacker Causeway, Miami, FL 33149, USA

^bAlfred Wegener Institut for Polar and Marine Research, PO 120161, 27515 Bremerhaven, Germany

^cInstitut für Meereskunde an der Universität Kiel, Düsternbrooker Weg 20, 24105 Kiel, Germany

^dDepartment of Oceanography, University of Cape Town, 7701 Rondebosch, South Africa

^eAtlantic Oceanographic and Meteorological Laboratory, National Oceanic and Atmospheric Administration, 4301 Rickenbacker Causeway, Miami, FL 33149, USA

^fWoods Hole Oceanographic Institution, MS 29, Woods Hole, MA, 02543, USA

^gNaval Research Laboratory, Stennis Space Center, MS, 39529, USA

Received 24 January 2002; accepted 27 July 2002

Abstract

Rings shed at the Agulhas retroflection are an integral part of interoceanic exchange south of Africa. There is clear evidence of westward ring translation from the northern Cape Basin across the South Atlantic Ocean. Early ring development and translation from the southern to the northern Cape Basin, however, are obscured by an intensely variable kinematic field close to the spawning site. In this study unique in situ observations, obtained in March to September 1997, are analyzed to improve the understanding of the early development of a juvenile Agulhas Ring. In March the ring was surveyed near 37°S, 16°E, approximately 4 months after its generation. Its strength and size were in the upper range typical for Agulhas Rings, and its trapping depth extended down to at least 1600 dbar according to geostrophic velocities and RAFOS trajectories in the ring. Between March and September the ring propagated in a general northwestward direction; however, RAFOS trajectories and MODAS sea-surface steric height fields revealed a large variability of the translation speed (3 cm s⁻¹ to more than 20 cm s⁻¹) and direction. In September 1997, the mature ring was examined near 31°S, 9°E. By this time, its available heat and salt anomaly were reduced by about 30% and its available potential energy was reduced by about 70%. This indicates that a significant loss of the ring characteristics occurred on the way from the southern to the northern Cape Basin. One-third of this loss is due to changes at intermediate depth (between 800 and 1600 m).

Published by Elsevier Science Ltd.

1. Introduction

Current concepts of the global thermohaline circulation place considerable emphasis on inter-

oceanic exchanges of water masses, such as the Indonesian throughflow and the Agulhas leakage south of Africa (Gordon, 1986). The transport of water from the South Indian to the South Atlantic Ocean has substantial implications for the convective circulation of the Atlantic Ocean as a whole (Gordon, 1985). Weijer et al. (1999) have

*Corresponding author. Fax: +1-305-361-4412.

E-mail address: claudia.schmid@noaa.gov (C. Schmid).

demonstrated that these interbasin fluxes of heat and salt are important for maintaining the strength and operation of the Atlantic thermohaline overturning.

The interoceanic exchange south of Africa is currently thought to consist of three major parts (Lutjeharms, 1996; de Ruijter et al., 1999): the advection of Agulhas filaments, the shedding of Agulhas Rings, and the transport of intermediate water between the two subtropical gyres in the Indian and Atlantic Ocean. The contribution of Agulhas filaments is significantly smaller than the contribution of Agulhas Rings. For the former the salt flux is only 12% of the flux associated with Agulhas Rings (Lutjeharms and Cooper, 1996).

Agulhas Rings are formed south of Africa where the Agulhas Current retroflects (Fig. 1; Lutjeharms and van Ballegooyen, 1988). The current loop created in this way is occasionally occluded so that a distinct ring of Agulhas water is shed into the South Atlantic Ocean (Lutjeharms and Gordon, 1987). These rings carry significant amounts of heat and salt from the Indian Ocean to the interior of the Atlantic Ocean.

After having been shed, Agulhas Rings may be closely bunched in the eastern Cape Basin, just north of the Agulhas retroflexion (Goñi et al., 1997; Duncombe Rae, 1991; Duncombe Rae et al., 1996). They are in fact the major cause of current variability in this region (Garzoli et al., 1996). Having moved to the western part of the Cape Basin, some may eventually move across the full width of the South Atlantic (Byrne et al., 1995), but recent analyses have shown that rings lose up to 50% of their energy in the Cape Basin (Schouten et al., 2000). Even more important is the finding that about one-third of all rings never leave this basin but seem to disintegrate completely in this turbulent region. This may be partially due to interaction with other rings and with cyclones (Lutjeharms et al., 2003), but some theoretical work has suggested that the bathymetry also may play an important role in this dissipation (Kamenkovich et al., 1996; Beismann et al., 1999). Arhan et al. (1999) and Schouten et al. (2000) have shown that rings may split at distinct seamounts that lie in their path. Such splitting may conceivably enhance the rate of ring dissipation, but

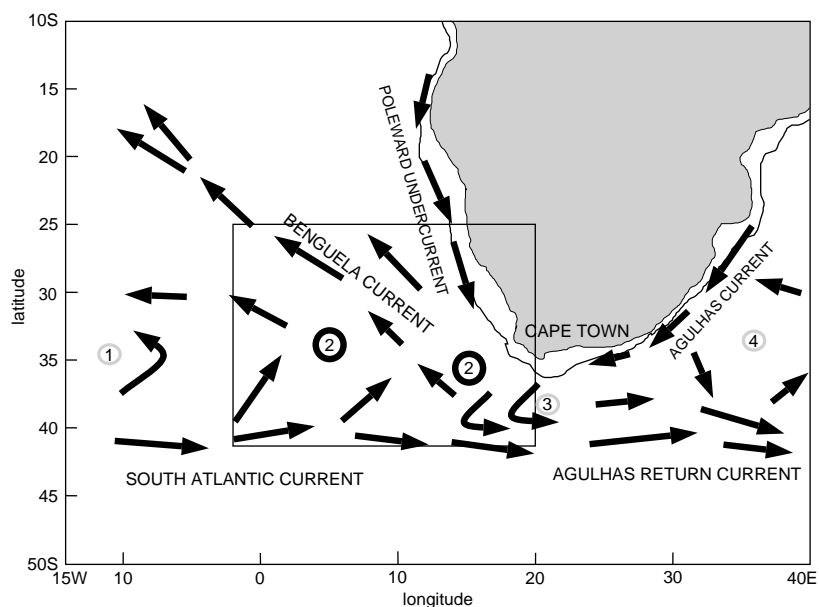


Fig. 1. Schematic of the intermediate depth flow around the tip of South Africa based on suggestions by Shannon and Nelson (1996), Reid (1989) and others. The African continent is shaded, and the line roughly parallel to the coast represents the 1000 m isobath. The numbered anticyclonic features are (1) the Subtropical gyre of the South Atlantic, (2) Agulhas Rings, (3) the Agulhas Retroflexion and (4) the Southwest Indian Ocean sub-gyre. Adapted from Boebel et al. (1998). The box indicates the region shown in Fig. 2.

the exchange processes of rings with the ambient waters at intermediate depths and with other rings and cyclones, even without the intervention of the bottom topography, are as yet not known.

Several issues are therefore important for the estimation of the manner in which Agulhas Rings contribute to interoceanic fluxes. These naturally include their horizontal and vertical dimensions as well as their anomalous heat and salt contents soon after having been spawned. For specific rings these values have been obtained by one-time hydrographic surveys (e.g., van Ballegooyen et al., 1994). But they do not allow a reliable quantification of how the flux into the interior of the Atlantic is affected by mixing or possibly by interaction with other mesoscale features at various depths during the rings' lifetime. This is particularly true for their sojourn in the Cape Basin where considerable mixing has been suggested (see Boebel et al. (2003b), for a review and new results). One way to address this problem would be to track a ring with altimetry and Lagrangian floats, the latter at a number of depths, and to measure its hydrographic properties. Such measurements could supply important information on the trapping depth of rings, their rate of decay as well as the exchange of water between rings and the surrounding water. This approach was taken during the international program KAPEX (Cape of Good Hope Experiment), which was initiated in 1997 (Boebel et al., 1998b; Lutjeharms et al., 1997).

We report here on a specific Agulhas Ring that was first observed during the initial cruise undertaken in March/April 1997 in the framework of the South Atlantic Current component of the KAPEX program. This ring was subsequently tracked by satellite altimetry and RAFOS trajectories, and revisited after a period of 5 months. The changes of the properties of this ring will be analyzed and the underlying causes will be discussed.

2. Data and methods

Data from two cruises were available for this study. The first KAPEX cruise started in Cape Town on 21 March 1997 (Boebel et al., 1997). A

following cruise began in Cape Town on 4 September of the same year (Garzoli et al., 1999). The segments of the cruise tracks that are of interest in this study are presented in Fig. 2.

In search for an Agulhas Ring, a shipboard ADCP and XBTs were used in March 1997. After detection of Agulhas Ring A near 16°E, 37°S five RAFOS floats were deployed. Prior to each RAFOS float deployment a CTD cast to depths between 1500 and 2000 m was taken. The initial drift depths of the RAFOS floats were then chosen to coincide with the local core depth of the Antarctic Intermediate Water (AAIW) layer.

The CTD data of this first cruise were obtained with a Neil Brown MKIIB instrument. Pre- and post-cruise calibrations of the temperature and pressure sensors were used for the correction of the measurements (Müller et al., 1995). The salinity corrections were based on reference salinities determined from water samples taken regularly with a rosette. The applied corrections yielded an overall accuracy of 0.002 psu for the bottle salinities. The fully calibrated data match WOCE standards.

The ADCP data were obtained with a vessel-mounted 153.6 kHz RDI instrument. After calibration and editing the data, the errors were estimated to be 8 cm s^{-1} for the cross-track component and 6 cm s^{-1} for the along-track component. The data were averaged into 25 m thick layers between 25 and 400 m.

The September cruise was part of the Benguela Current Experiment, and its hydrographic results have been described in detail by Garzoli et al. (1999). During this cruise 30 RAFOS floats were launched equidistantly along 30°S and 7°W in order to measure directly the intermediate depth flow in the northern Cape Basin. Three Agulhas Rings were identified by Garzoli et al. (1999). The easternmost of them was named ring 1. We will show that this ring is identical with ring A observed in March 1997. From here on we will refer to ring 1 as ring A.

A subset of the obtained Lagrangian data is presented in Fig. 2. The March data set consists of trajectories from five RAFOS floats in ring A (near 16°E), and a CTD/ADCP section through the ring. The September data set contains trajectories from

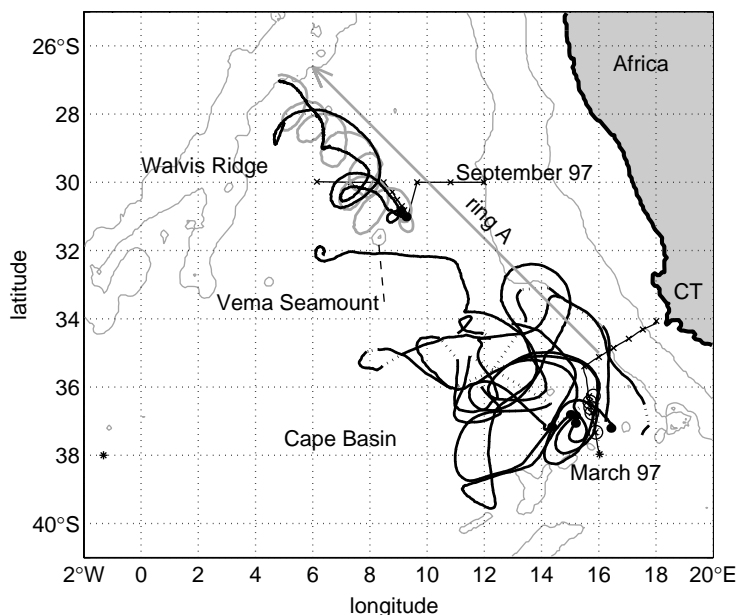


Fig. 2. Trajectories of RAFOS floats (black) and a surface drifter (gray) deployed in March (near 16°E, cruise R/V *Polarstern* ANT XIV/4) and September 1997 (near 9°E, R/V *Seward Johnson*). The long gray vector labeled ring A at 31°S, 11°E indicates the translation of the ring. Segments of the cruise track in the vicinity of the deployment are shown. Crosses mark CTD stations, and circles indicate the deployment positions of the RAFOS floats launched in March 1997. The asterisk at 38°S, 1°W denotes the position of the reference profile for pure South Atlantic water used to estimate the bulk properties in Table 1. The asterisk at 38°S, 16°E indicates the position of the profile used in Fig. 10. The isobaths are at 1000 and 4000 m. CT indicates Cape Town.

two RAFOS floats and two surface drifters in ring A (near 9°E).

During both cruises, quasi-isobaric RAFOS floats were used, which are neutrally buoyant instruments that drift freely with the surrounding water (Rossby et al., 1986). Their underwater navigation is derived from the travel times of coded sound signals which were emitted twice daily from several sound sources. In addition, they record the temperature and pressure on an identical schedule. The qualifier “quasi-isobaric” is used for floats that exhibit a more isobaric behavior than an isopycnal float. However, the former do not stay on a given isobar (such a behavior would require active volume control). Instead they follow vertical motions of their environment only by order of 30–50% of the corresponding water parcel’s vertical excursion (since they are less compressible than water). This behavior must be taken into account when interpreting the RAFOS trajectories with regard

to water exchange, especially in the presence of fronts with strong inclinations. An important tool is that the salinity of the water around a RAFOS float can be estimated from the temperature and pressure records via the equation of state of the float and the equation of state of sea water (Boebel et al., 1995). This information permits the identification of transitions from one water mass to another.

Surface steric height fields will be used in an effort to interpret individual RAFOS trajectories in the context of the mesoscale flow field at the sea surface. The steric height data were provided by the Naval Research Laboratory and Naval Oceanographic Office at Stennis Space Center. Their Modular Ocean Data Assimilation System (MODAS; Carnes et al., 1996) produces global 1/8° resolution maps of sea-surface steric height relative to 1000 m. Here, steric height is the difference in the height of a given water column and the height of an ideal 0°C, 35 psu column at

rest. The heights are integrated between specified pressure surfaces. The estimation of the steric height begins with optimal interpolation of TOPEX and ERS2 altimetry, which uses a mesoscale-tuned estimate of the error covariance to develop a field of deviations from the mean height (Jacobs et al., 2001; Fox et al., 2002). The final steric height is produced by adding the deviation field to two others, a MODAS climatological mean steric height and a correction for the difference between the altimetric and climatological means. The climatological steric height is computed by integrating from the climatological pressure at 1000 m to the surface (for more details, see <http://www7300.nrlssc.navy.mil/altimetry>). A comparative analysis of MODAS geostrophic velocities and in situ velocity observations performed by Boebel and Barron (2003) yields high correlation coefficients for the flow direction (0.8–0.9). The combination of MODAS steric height and float trajectories is used throughout this publication, but primarily in Section 3.3 to establish that the same ring was encountered in March and September.

3. A juvenile Agulhas Ring

3.1. Hydrographic properties

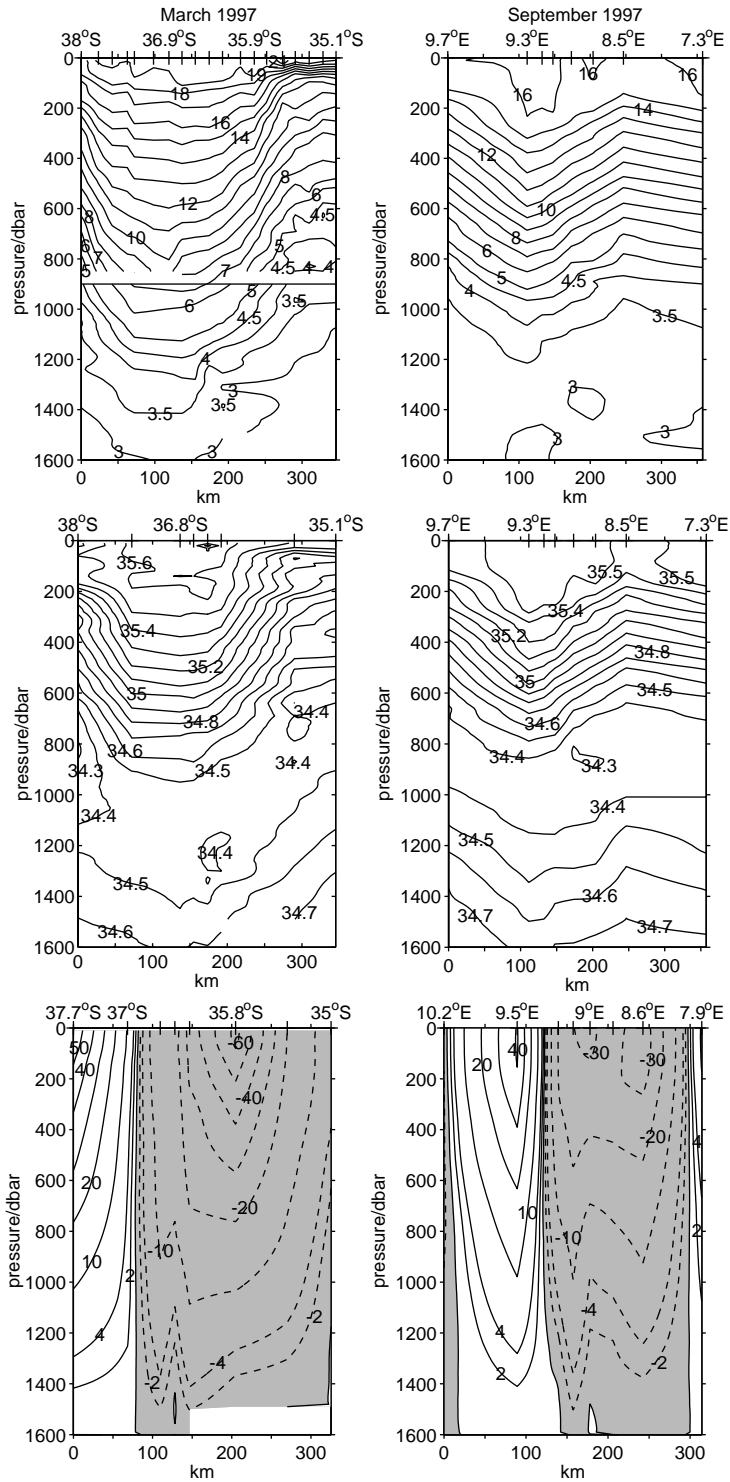
Between 22 and 24 March 1997, R/V *Polarstern* crossed a regime of enhanced sea-surface temperatures and salinities (Fig. 3, left panels). Along the section the 10°C isotherm deepened from 200 dbar at 35°S to 800 dbar at 36.9°S before rising again. This is indicative of an anticyclonic circulation pattern and typical for Agulhas Rings. The velocity measured with a shipboard ADCP is consistent with such a circulation, it was westward at the northern and eastward at the southern end of the section (Fig. 4). However, these observations alone are insufficient to identify an Agulhas Ring since the cruise track could have crossed the Agulhas Retroflection rather than an Agulhas Ring. But the first presumption is supported by satellite and Lagrangian data: the strong positive anomaly in the steric height field indicates that closed streamlines are likely to exist, and the RAFOS trajectories clearly show the expected

anticyclonic looping during late March through mid-June (Fig. 5, note that the ring is always in the center of the panels). All these observations corroborate the conjecture that the cruise track transected an Agulhas Ring (which was named ring A).

In the Antarctic Intermediate Water layer the salinity increased towards the ring center (from less than 34.4 psu outside of ring A to just below 34.5 psu nearly everywhere inside the ring, Fig. 3, left). This clearly demonstrates the strong influence of the more saline water from the Indian Ocean. For a quantitative examination of this influence it is necessary to derive the bulk properties and their change over time. Two hydrographic sections will be used for this purpose (Fig. 2).

A CTD profile obtained in March 1997 at 38°S, 1°W (indicated by an asterisk in Fig. 2) was chosen as a reference profile for the calculation of the bulk properties. Velocity observations taken during the cruise indicate that this profile was obtained just north of the maximum speed core of the eastward South Atlantic Current (Boebel et al., 1998a), which transports water from the western Atlantic into the Cape Basin. Consistent with this the hydrographic data obtained during the cruise also provide evidence that the profile is in the Subtropical Front (Boebel et al., 1998a), which is closely linked to the South Atlantic Current. Steric height fields (not shown) also support the position of the profile relative to this current. The choice of this reference profile was motivated by the following consideration: If the input of Indian Ocean water into the Cape Basin could be turned off, then the water properties in this basin would be well represented by this profile, which is located southwest of the region that is influenced by Indian Ocean water. Therefore, the chosen profile is well suited as a reference for the estimation of the anomalies associated with Agulhas Rings, and their effects on the Atlantic water masses.

Additional assumptions are that the ring is circular and that its radius is 90 km (within which the anomalous water was found during both surveys). Based on these assumptions available potential energy and available heat and salt anomalies are computed along isopycnals (bounded by potential density surfaces).



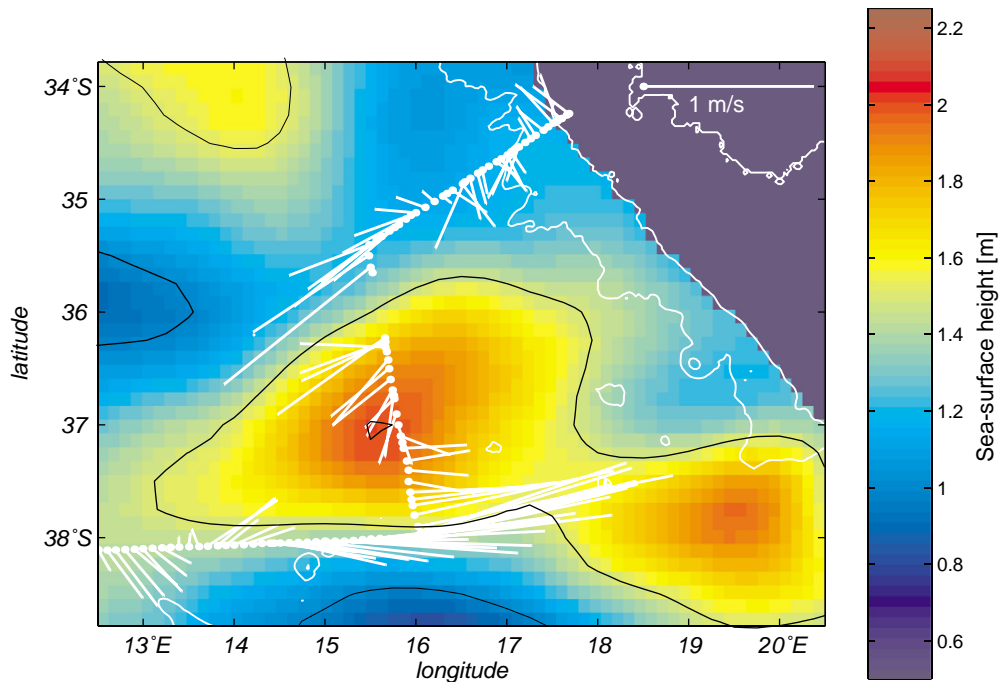


Fig. 4. Velocities from ship-board ADCP in the 25–50 m layer on top of MODAS steric height for 23 March, 1997. The center of ring A is near 37°S, 16°E. The black contour lines indicate 1, 1.5 and 2 m.

For the remainder of this section the focus will be on the March survey. In Section 3.2 (below) we show that the cruise track came close to the ring center. The smallest distance was about 25 km, which allows a quite accurate computation of the bulk properties of ring A. This statement is based on two facts. The small distance between the section and the ring center leads to an underestimation of the ring radius by only 4% (based on the 90 km derived above), and the water properties within the ring's core (i.e. within 25 km from its center) do not change much. The assumption of a circular ring is supported by the initial RAFOS trajectories in conjunction with the steric height field (Fig. 5, 2 April 1997). During the cruise the ring appears to be less circular in the steric height

field (Fig. 5, 23 March 1997), but this impression is primarily due to the outer fringes of the ring. The core region (where the anomalies are largest) is nearly circular.

Three vertical integration limits were used: 800, 1100 and 1600 dbar (i.e. none of the isopycnal layers used in the computation may extend to higher pressure than the respective integration limit). The smallest pressure represents the maximum depth of the 10°C isotherm in March. The pressure of 1100 dbar corresponds to the minimum trapping depth indicated by the RAFOS data (two floats were very close to this pressure surface and experienced vigorous anticyclonic drifts). The largest pressure corresponds to the maximum common pressure of the profiles near



Fig. 3. Two sections through ring A are shown (for cruise tracks see Fig. 2). The left and right panels show the March 1997 and the September 1997 data, respectively. Temperature in degrees Celsius (top), salinity in psu (middle), geostrophic velocity relative to 1600 dbar in cm s^{-1} (bottom). Note that the horizontal resolution in the temperature section for March changes at 900 dbar (indicated by a black line; the shallower part includes XBT profiles).

the ring center, where the anomalies are still clearly visible in the sections (Fig. 3).

For March the available heat and salt anomalies were 1.44×10^{20} J and 9.5×10^{12} kg in the upper 800 m, respectively (Table 1). The corresponding available potential energy of the ring amounted to 11.2×10^{15} J and the volume was 20×10^{12} m³. These anomalies are near the high end of those derived for other Agulhas Rings (with

similar vertical integration limits; e.g., McDonagh et al., 1999). The bulk properties of ring A increase significantly with the integration depth. The contribution of the 800–1600 m layer (which includes the AAIW) to the heat and salt anomalies associated with ring A was about 32% and 21%, respectively. Half of this intermediate depth contribution is due to the 800–1100 m layer.

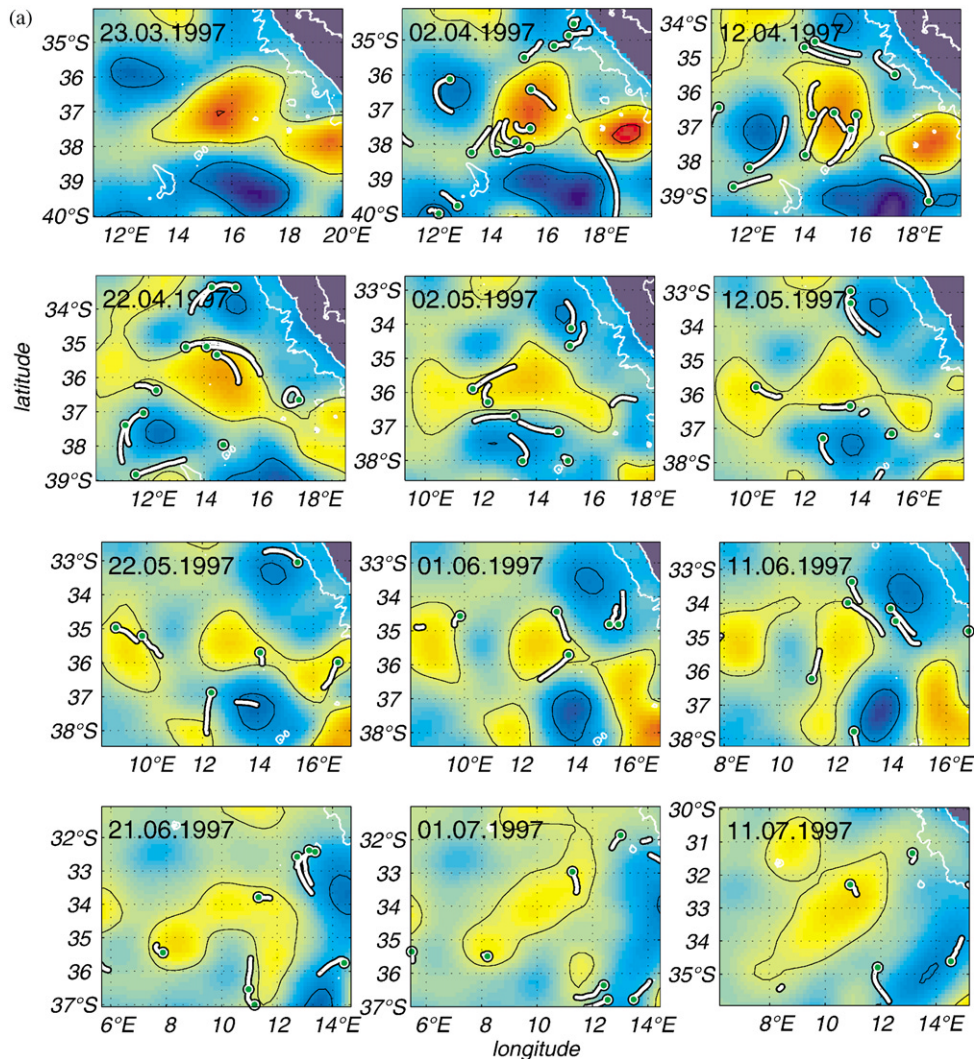


Fig. 5. MODAS steric height and RAFOS trajectories. The trajectories are for a period of ± 3 days around the date of the steric height anomaly field. Note that the axis is panning with the eddy, i.e. ring A is always in the center of each map. The March trajectories have a green head and the September trajectories have a magenta head. The colors and the black contour lines are the same as in Fig. 4.

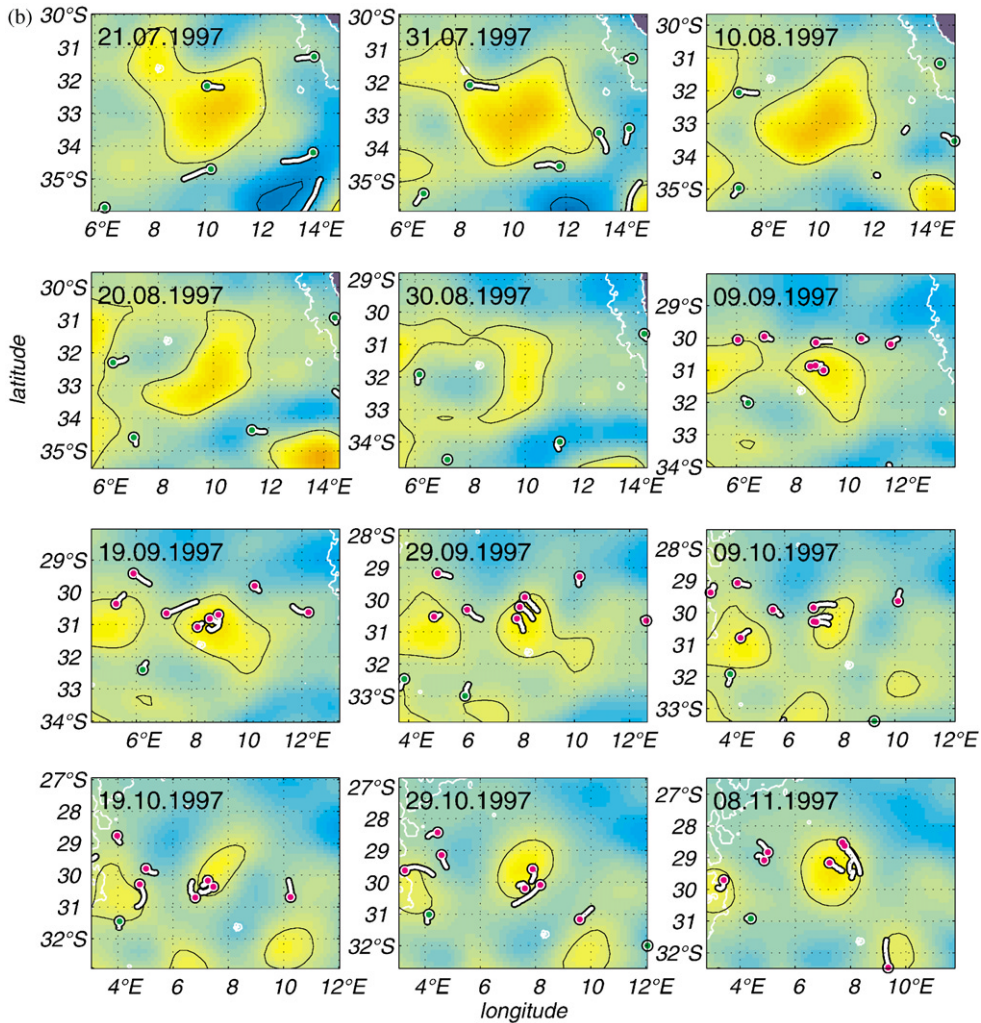


Fig. 5 (continued).

3.2. Kinematic properties

The ship-board ADCP measured high speeds north and south of a speed minimum in the 25–50 m bin (Fig. 4). The speed decreased from 78 cm s^{-1} at 36.2°S to less than 24 cm s^{-1} around 37°S and increased again to 86 cm s^{-1} at 37.7°S and 153 cm s^{-1} at 37.9°S . The longest vectors were nearly perpendicular to the section and pointed in nearly opposite directions in the two high-speed regions. The speeds adjacent to the minimum at 37°S were 31 cm s^{-1} at 36.9°S and at 37.1°S (they were obtained within an interval of only 2 hours

on 23 March). The directions change significantly from south-southwest (200°) to south-southeast (160°) and finally to east-southeast (110°) over a distance of about 25 km. This indicates that the ring center must have been close to the section, which allows a relatively accurate estimate of the center's location. Using the three velocity observations closest to the ring center (see above) and the assumption of a circular ring the location of the ring center is derived as $36.90^\circ\text{S} \pm 0^\circ$, $15.97^\circ\text{E} \pm 0.04^\circ$ (which is 25 km away from the section). The latitude agrees well with the latitude derived from the steric height field for 23 March (Table 2), but

Table 1
Bulk properties of an Agulhas Ring

Bulk property	March 1997	September 1997	Reduction (%)	Integration depth (m)
AHA (10^{20} J)	1.44	1.14	21	800
AHA (10^{20} J)	1.71	1.33	22	1100
AHA (10^{20} J)	2.13	1.47	31	1600
ASA (10^{12} kg)	9.5	7.3	23	800
ASA (10^{12} kg)	10.7	8.0	25	1100
ASA (10^{12} kg)	12.1	8.4	31	1600
APE (10^{15} J)	11.2	5.6	50	800
APE (10^{15} J)	17.5	8.1	54	1100
APE (10^{15} J)	24.9	7.8	69	1600
Vol (10^{12} m ³)	20	20	—	800
Vol (10^{12} m ³)	28	28	—	1100
Vol (10^{12} m ³)	41	41	—	1600

AHA is the available heat anomaly, and ASA is the available salt anomaly. APE is the available potential energy. The bulk properties are estimated for a reference profile at 38°S, 1°W (it is marked with a star in figure) and a ring radius of 90 km (this radius is prescribed by the outermost profile that still reveals hydrographic anomalies). Column four gives the reduction of the bulk properties over the 5-month period. The last column gives the integration depth. The approximate volumes (Vol) for the three integration depths are given in the last three lines.

the longitude is nearly 0.5° farther east. This difference is insignificant for two reasons. First, the errors of the estimated center positions from the steric height fields are about 1/4°, which reduces the discrepancy by 50%. Second, the steric height represents a 10-day average whereas the position derived from the velocities is based on a synoptic survey.

The geostrophic velocity relative to 1600 dbar reveals the vertical structure of the speed down to intermediate depths (Fig. 3, bottom panels). The sections show the deep-reaching cores of west- and eastward flow on opposing sides of the ring center. In March (Fig. 3, bottom left) the velocity decreased rather rapidly at about 10 cm s⁻¹ per 200 dbar between the surface and 1000 dbar. Below this depth the decrease was considerably weaker.

The choice of the level of no motion at 1600 dbar is a compromise that allows a presenta-

Table 2
Date, positions, translation speed and direction of ring A from MODAS steric height fields at 10-day intervals

Date	Latitude	Longitude	Speed (cm s ⁻¹)	Direction
23.3.1997	-37.03	15.50	1.7	243
<i>Period 1:</i>				
2.4.1997	-37.10	15.35	6.5	346
12.4.1997	-36.60	15.20	9.7	320
22.4.1997	-36.02	14.60	10.3	303
<i>Period 2:</i>				
2.5.1997	-35.59	13.77	4.8	279
12.5.1997	-35.53	13.32	4.8	279
22.5.1997	-35.46	12.87	3.3	284
1.6.1997	-35.40	12.57	3.4	315
<i>Period 3:</i>				
11.6.1997	-35.21	12.34	27.3	302
21.6.1997	-34.07	10.17	2.5	288
1.7.1997	-34.01	9.94	15.7	31
<i>Period 4:</i>				
11.7.1997	-32.96	10.70	3.5	265
21.7.1997	-32.98	10.38	1.1	46
31.7.1997	-32.92	10.45	3.3	14
10.8.1997	-32.67	10.53	5.2	288
20.8.1997	-32.54	10.07	9.7	350
30.8.1997	-31.80	9.92	8.7	325
9.9.1997	-31.24	9.47		

The error in the estimate of the center position is about 1/4°, which corresponds to about 3 cm s⁻¹.

tion of data from both cruises based on the same assumption. This reference level, however, leads to an underestimation of the velocity in March. The near-surface ADCP (Fig. 6) and the initial RAFOS speeds at intermediate depth (Table 3) were higher than the geostrophic velocities. Such differences can be reduced if the barotropic component of the velocity is known. The ADCP velocities could not be used to derive the barotropic component throughout the section because of gaps along the cruise track. Only for five profiles (out of eight) a comparison in a layer extending from 25 m to at least 150 m was possible.

The results from the comparison for the five profiles are: at and north of the latitude of the ring center the barotropic cross-track velocity is always less than 10 cm s⁻¹. In fact, for the two profiles

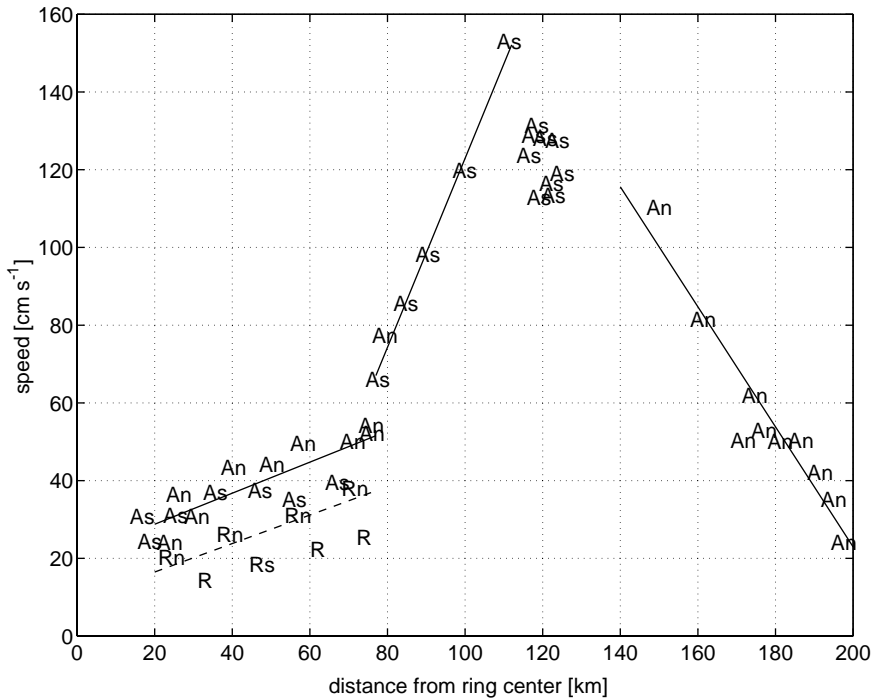


Fig. 6. Speed as a function of the distance from the center of ring A. The letters An (As) indicate ADCP observations between 25 and 50 m north (south) of the ring center. The letters Rn (Rs) indicate the initial RAFOS velocity values north (south) of the ring center. The letters R indicate swirl velocities for the first full revolutions of RAFOS floats. The solid (dashed) lines are linear fits to ADCP (RAFOS) data inside a range of distances from the ring center.

Table 3

Initial speeds of RAFOS floats (from launch position to first under water position fix, column three), in 800–1100 dbar, and distance between launch position and the center of ring A (column four, this position was derived from the ADCP data obtained in March 1997)

RAFOS (#)	Time (days)	Speed (cm s ⁻¹)	Distance (km)	Coriolis parameter (s ⁻¹)	Rossby number	Leaving ring A	Pressure (dbar)
183	5.6	38.1	71.6	-8.697e-05	0.06	3 April	1051
184	4.3	20.3	24.4	-8.747e-05	0.10	22 April	819
200	3.5	30.9	56.9	-8.714e-05	0.06	27 April	1028
215	3.4	26.1	39.4	-8.732e-05	0.08	4 June	1024
216	3.6	18.3	47.7	-8.805e-05	0.04	17 April	874

The second column gives the elapsed time from the launch time to the first position fix. Columns five and six give the associated Coriolis parameter and the Rossby number. Column seven gives the first date a RAFOS float left ring A (i.e. ignoring the recapturing of RAFOS floats). The first recorded pressure is given in the last column.

closest to the ring center it is less than 2 cm s⁻¹ (this increases our confidence in the earlier estimate of a 25 km distance between the section and the ring center, since the speed should be

nearly zero in the ring center). The percentage of the barotropic component does not exceed 22%. It has to be cautioned here, however, that the ADCP velocities are close to the measurement error (see

Section 2). South of the ring center the barotropic component becomes much more important (note that a comparison is only possible for the profile at 37.7°S), with more than 30 cm s⁻¹ (about 40% of the total velocity). This may be partly due to the South Atlantic Current or due to eddy–eddy interactions (see Section 4.3). These results are similar to those of Clement and Gordon (1995), who used a reference level of 1500 dbar and concluded that as much as 50% of the flow in their eddies is barotropic.

At intermediate depth the initial speed of the RAFOS floats was typically 20 cm s⁻¹ or more, with one exception. In many cases the initial speed was also about 20 cm s⁻¹ larger than the velocity derived from the nearest geostrophic profile. Two examples are RAFOS 215 with 26 cm s⁻¹ versus 8 cm s⁻¹ and RAFOS 200 with 31 cm s⁻¹ versus 10 cm s⁻¹. Even so these differences cannot be used to correct the geostrophic velocities by adding them as a barotropic component (since the RAFOS velocities are point measurements) they imply that the velocity between 1000 and 1600 dbar most likely exceeds 20 cm s⁻¹ in the high-speed regions of the ring. This in turn suggests that the trapping depth may be least 1600 dbar, which agrees well with the observed hydrographic anomalies (Fig. 3).

The near-surface radius–speed relationship is quite interesting. The speed increased nearly linearly from 30 cm s⁻¹ at a radius of 20 km to 50 cm s⁻¹ at 80 km (Fig. 6). From 80 to 110 km a much stronger linear increase from 70 to 150 cm s⁻¹ is evident (this maximum was observed south of the ring center). The subsequent decrease at radii greater than 150 km (starting at 110 cm s⁻¹) was nearly as steep as the increase. No observations are available at the radius where the maximum speed north of the ring center is expected (because the ADCP did not work between 80 and 150 km). It is noted, however, that the linear decrease is based on measurements north of the center. If we assume that its slope is representative down to a radius of 110 km, then the maximum speed in the north is also 150 cm s⁻¹. The speed–radius relationship observed here is not typical for isolated eddies, which indicates that other mesoscale features may interact with ring A.

The steric height fields are useful for understanding the change of the speed–radius relationship near 80 km. The map for 23 March (Fig. 5) shows a strong cyclone south of ring A. The distance between the two eddy centers is only about 250 km, which is not much larger than the sum of the eddy core radii (which are on the order of 100 km). If two eddies are in such close proximity, they can be viewed as a dipole (Flierl, 1981), and the speed between them is higher than the maximum swirl speed of equivalent isolated eddies. (Such dipoles occur frequently in this region, but they are short-lived since the anticyclones and cyclones propagate in different directions; Boebel et al., 2003a.) This eddy–eddy interaction strongly affects the velocity structure of both eddies, which prevents an estimation of the maximum swirl speed and the associated core radius of ring A. When taking earlier observations of Agulhas Rings into account (e.g., Duncombe Rae et al., 1996; McDonagh et al., 1999), one can conclude that the most likely range for the radius of maximum swirl speed is 80–120 km.

3.3. Ring translation

In the steric height fields (Fig. 5) the positive anomaly associated with ring A can be tracked from the site of its first hydrographic survey southwest of Cape Town to the site of the second survey near Vema Seamount (Fig. 2). The translation of ring A was divided into four periods (Table 2). The first period covers the 2 April–2 May panels of Fig. 5. During this time ring A translates in a northwestward direction from 37.1°S, 15.4°E to 35.6°S, 13.8°W (Fig. 7) at speeds ranging from 6 to 11 cm s⁻¹.

The second period began in early May when the intensity of the positive anomaly of ring A in the steric height fields started to wane (Fig. 5). The ring translated northwestward by approximately one ring diameter to 35.2°S, 12.3°E on 11 June (Fig. 7) at rather low speeds between 3 and 5 cm s⁻¹ (Table 2).

This period of relative stability and quiescence was succeeded by a third period of vigorous translation and merging. The highest translation speed during this period is about 27 cm s⁻¹, and

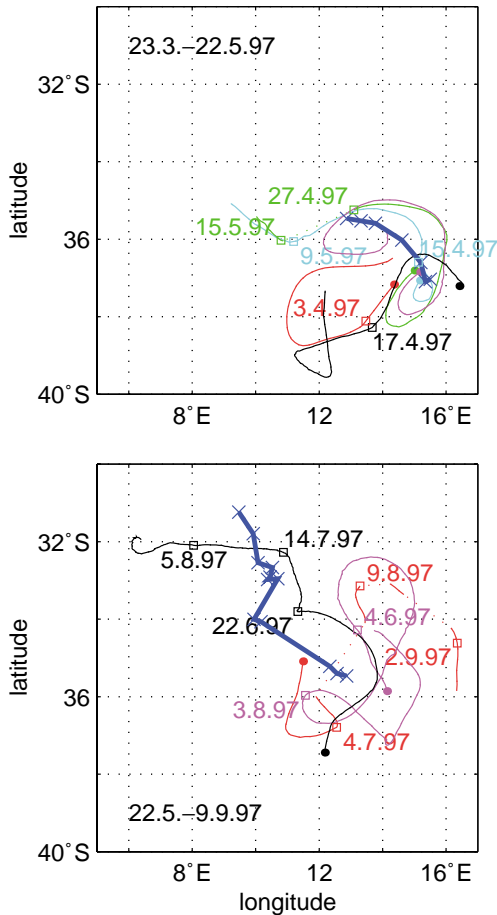


Fig. 7. Trajectories of RAFOS floats that were in ring A for part of their mission (red: #183; cyan: #184; green: #200; magenta: #215; black: #216). Squares indicate the positions corresponding to the dates. Dots mark the start of each trajectory. The positions of the steric height anomaly associated with ring A are indicated by the thick blue line with crosses.

the average is about 15 cm s^{-1} . The 27 cm s^{-1} seem somewhat high, but even if one assumes a position error of $\frac{1}{4}^\circ$ for both positions used to derive this speed the result is still large (about 21 cm s^{-1}). The frequent changes of the translation during this period may be due to strong eddy–eddy interactions: On 11 June a smaller positive anomaly to the south came close to ring A. Ten days later a western positive anomaly also was close to ring A. In the following 20 days the

smaller anomalies disappeared, which suggests that they may have merged with ring A and formed an anomaly of ellipsoidal shape. This process was probably responsible for the termination of the westward translation of ring A at 10°E .

The last, calmer period began in early July, when the anomaly strengthened again and reorganized itself from the ellipsoid shape into a more circular shape. During this process ring A translated slowly north along 10°E . Translation speeds commenced around 3 cm s^{-1} , but reached higher values around 9 cm s^{-1} during the last two 10-day periods. In early September 1997 ring A was found near 31°S , 9°E during the second hydrographic survey.

The translation of ring A also was derived from the RAFOS trajectories. Around 5 April the ring center was near 37.3°S , 15.3°E (Table 4), which is 74 km southwest of the position derived from the March survey (36.90°S , 15.97°E). The translation over about 14 days corresponds to an initial translation speed of 6 cm s^{-1} . The uncertainty of the translation is mirrored in the locations derived from RAFOS 200 and RAFOS 215 for about the same time (27 March to 15–17 April). The distance between the two location estimates is about 35 km , which is nearly half of the distance covered in the 14-day period. The corresponding error of the translation speed is about 3 cm s^{-1} . From 5 April to 12 May the translation speed was about 7 cm s^{-1} towards the northwest (again with an error of 3 cm s^{-1}), which matches the speed derived from the steric height fields ($8 \pm 3 \text{ cm s}^{-1}$ to the northwest for 2 April–12 May, Table 2). The $6 \pm 3 \text{ cm s}^{-1}$ to the southwest for the earlier period are larger than the value derived from the steric height fields ($2 \pm 3 \text{ cm s}^{-1}$ to the southwest for 23 March–2 April), but the difference is well inside the error bounds.

4. Discussion

4.1. Water properties and the origin of ring A

The inter-oceanic exchange associated with an Agulhas ring is governed by three factors: (a) the ring's initial hydrographic composition, which is

Table 4

Center, radius and speed for trajectory segments (only full revolutions) of RAFOS floats in 800–1000 dbar and a surface drifter

	Date	Latitude (°S)	Longitude (°E)	Radius (km)	Speed (cm s ⁻¹)	Rosby number
<i>RAFOS (#)</i>						
184	28.3.–12.4.1997	37.3	15.3	33±9	14.4±2.8	0.05
200	27.3.–17.4.1997	37.6	14.9	74±25	25.3±7.5	0.04
215	27.3.–15.4.1997	37.4	15.2	62±19	22.3±5.9	0.04
215	24.4.–30.5.1997	35.9	13.3	81±14	16.6±9.2	0.02
383	11.9.–21.9.1997	31.0	8.8	19±4	14.4±4.0	0.10
383	1.10.–2.11.1997	30.2	7.3	65±13	15.4±4.3	0.03
390	5.10.–24.10.1997	30.3	7.3	28±8	11.5±4.0	0.07
<i>Drifter (#)</i>						
19,845	14.9.–19.9.1997	31.1	9.2	14±2	21.7±5.0	0.21
19,845	24.9.–7.10.1997	30.9	8.0	64±17	36.8±13.8	0.08

Radius and speed are given with standard deviation.

closely linked to its generation site and date; (b) the ring's translation characteristics, in particular how quickly it separates from the Agulhas Retro-reflection; and (c) the intensity of mixing with the ring's environment. While the issue (c) is left for the following sections, we will here discuss the ring's origin and early kinematic characteristics and the closely related issue of its hydrographic properties. The overall close relationship between float trajectories and SSH anomalies as documented in the previous sections and in related studies (Boebel et al., 2003b; Lutjeharms et al., 2003) gives us confidence in an extrapolation of the steric height signal towards times before the floats were launched and hence to trace the dynamic signal of ring A back to its origin.

Steric height data for this region became available from 1 January 1997 onwards (Fig. 8). At this time a large 450 km long and 220 km wide ellipsoidal positive anomaly centered at 38°S, 18°W was observed to fill the ocean between the tip of the Agulhas Bank and the Agulhas Ridge. Similar asymmetric structures already have been noted by Olson and Evans (1986). They are the predecessors of the more circular Agulhas Rings found farther west. The Agulhas Retro-reflection had its westernmost edge along 21°W, just 3° east of a feature that can be associated with the ring A

found in March 1997 near 16°E. The pattern of the positive anomalies suggests that the spawning of ring A had occurred shortly before and we estimate the time of the first separation of ring A to be sometime in December 1996, a period for which no steric height data are available. Garzoli et al. (1999) used TOPEX/POSEIDON altimetry for backtracking and came to the conclusion that ring A was shed during February 1997. The steric height data with their higher resolution allowed to identify the earlier date for the ring shedding. A few weeks after the spawning of ring A, a second, smaller ring with a diameter of around 170 km diameter was occluded from the retro-reflection on 17 January (Fig. 8). This ring commenced to merge with ring A within 10 days. This process was completed by 3 February (Fig. 8). Throughout January, feature A, as described by the 1.5 m steric height contour, underwent dramatic morphological changes, occasionally developing internal structures of up to three sub-cores (Fig. 8).

The inferences from the kinematic field can be confirmed by analyzing the hydrographic section through ring A. The extent to which a ring displays the undisturbed (salt-enhanced and warmer) hydrographic characteristics of its constituent, the Indian Ocean water, is obviously dependent on the initial composition and subsequent intensity and

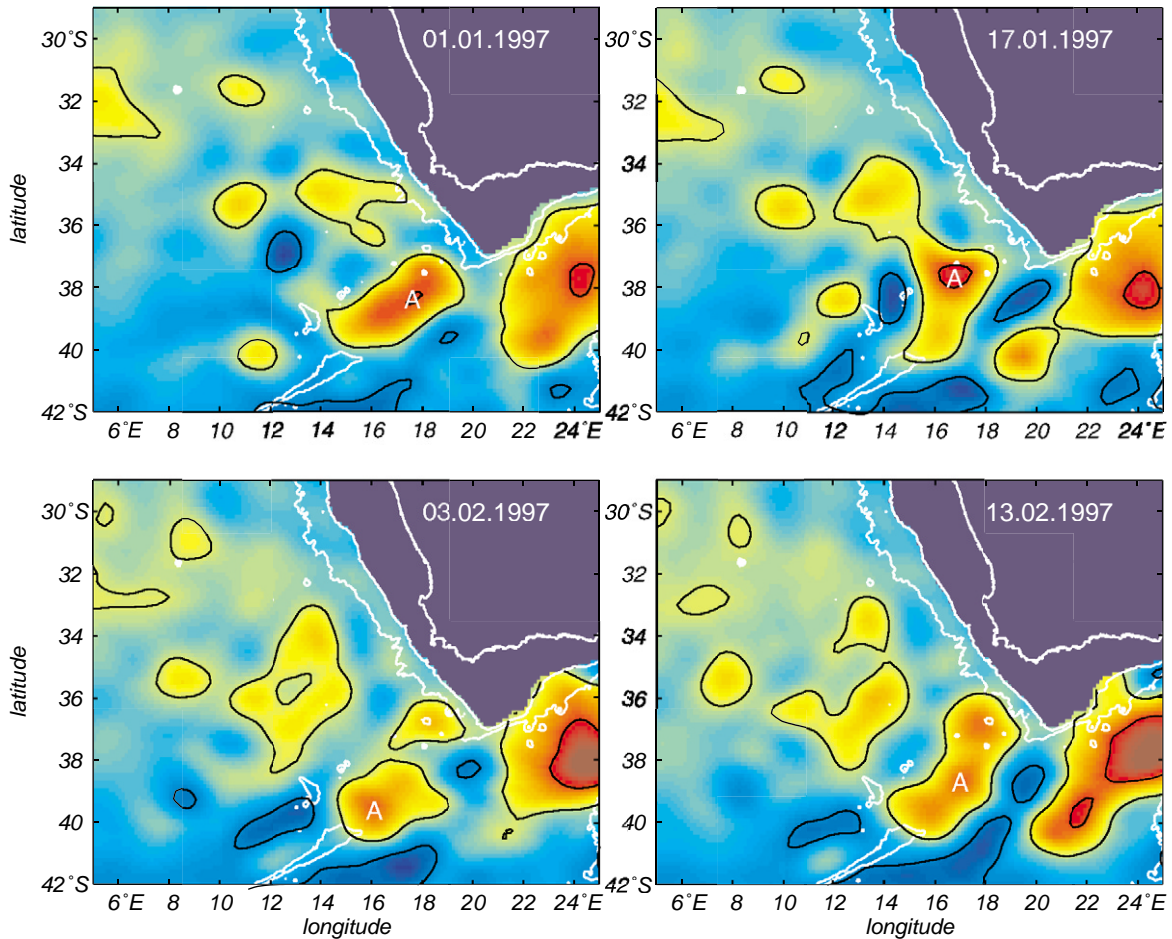


Fig. 8. MODAS steric height for four different times (starting at 1 January, the first time MODAS data are available). An “A” indicates the structure that can be associated with the ring A found in March 1997. The colors and the black contour lines are the same as in Fig. 4.

duration of mixing processes between the ring and its surrounding waters, as well as interactions with the overlying atmosphere. Generally, the younger a ring, the less diluted we expect its characteristics to be. In this case, with the presumed formation occurring in December 1996, we would expect to observe salt-enhanced and warm Indian Ocean water within the ring during the hydrographic survey of March 1997. The core salinity could have been augmented by less diluted Indian Ocean water due to the absorption of a second ‘younger’ ring in mid-January. The salinity within the ring’s perimeter could have been boosted by the most recent

reattachment to the Agulhas Retroflection in mid-March 1997.

Concerning the temperature distribution in Agulhas Rings past studies showed two distinctively different types rings: those with a thermostat layer, and those without such a layer (van Ballegooyen et al., 1994; Duncombe Rae et al., 1996; McDonagh et al., 1999; Arhan et al., 1999; Garzoli et al., 1999). Ring A contained a relatively salty core but lacked any sign of a thermostat in its center (Fig. 3). From this lack of homogenization, possible periods and locations of formation can be constrained.

One frequently observed thermostad (17.4–17.8°C) within Agulhas Rings is formed from South Indian Subtropical Mode Water (SIMW; Olson et al., 1992), which is found just below the seasonal thermocline. This water mass is formed in late austral winter and transported southward within the offshore (anticyclonic) segment of the Agulhas Current to become an integral part of the Agulhas Retroflexion loop. The lack of SIMW within ring A indicates that this water mass was not present during the ring formation and hence suggests its formation in austral summer. A formation prior to the austral winter 1996 also can be excluded since ocean–atmosphere exchange during winter would have generated a deep, well-mixed convective layer (Mey et al., 1990), which is not found in ring A. Therefore, the ring must have formed after July–September 1996.

The situation during formation and the ring's path can be constrained from the presence or absence of colder thermostads (e.g. 11–12°C, or 13–14°C), which are indicative for the entrainment of surface water originating south of the Subtropical Front (e.g. Subantarctic Surface Water). These thermostads are typical for deep convection at higher latitudes in the austral winter, and they usually have a high oxygen content (Arhan et al., 1999). Such water also can be found in the southwestern part of the Agulhas retroflexion region (Gordon et al., 1987; Valentine et al., 1993). The absence of such cold thermostads in ring A indicates that no intrusion of Subantarctic Surface Water took place during the ring formation and that ring A stayed north of the Subtropical Front after its formation. The latter also is supported by the ring's translation derived from the steric height maps. Therefore, no such cold mode water could be entrained into the ring as it propagated towards the Walvis Ridge.

By exclusion, these findings agree with the earlier inference that ring A is a young ring that was formed approximately 2 months into the austral summer, in December 1996, from an occlusion of the Agulhas Retroflexion loop.

While the ocean–atmosphere interactions modify the upper thermal structure, the intermediate layer is to a large extent sheltered from atmo-

spheric influences and hence could give a more undisturbed view of the ring's initial water masses. The hydrographic survey in March 1997 discloses that the Antarctic Intermediate Water (AAIW) in the core of the ring was largely composed of Indian Ocean AAIW; the salinity range in the ring was closer to the salinities observed in the western Indian Ocean (e.g., Shannon and Hunter, 1988) than to salinities in undiluted Atlantic AAIW. This is consistent with the trapping depth of at least 1600 m (as derived above). A clear contrast existed to the AAIW outside of the ring which apparently was strongly influenced by AAIW of Atlantic origin. This, again, suggests that the ring is likely to be young. However, the extent to which intermediate water from the Indian Ocean is trapped by and transported with Agulhas Rings is not well known. The changes of the water in the ring and the underlying processes will be discussed in the next two sections.

4.2. Changes of the properties of ring A during 5 months

Before comparing the initial hydrographic properties with those observed after the ring had lived through the austral winter and translated north, the location of the cruise tracks relative to the ring center has to be analyzed. The smallest distance between the section and the ring center derived from the steric height field was 38 km on 23 March and 33 km on 9 September. A second estimate for 23 March yields 25 km, based on the center position derived from the ADCP data (Section 3.2). These findings indicate that the distance between the ring center and the sections was about the same for both cruises, which allows a comparison of the properties along the two sections, and the derived bulk properties.

In March the sea-surface temperature exceeded 19°C whereas temperatures greater than 17°C had completely vanished in September (Fig. 3, top). At the same time the mixed-layer thickness increased two-fold. These changes are due to cooling in the austral winter. During the 5-month period the 10°C isotherm had shoaled from 800 to 630 dbar. The shoaling of the isotherms can be seen down to more than 1200 dbar, i.e. it continues below the

AAIW layer. The changes of the salinity distribution is qualitatively similar to the changes of the temperature distribution: The salinity decreases at the surface and in the AAIW layer, the isohalines are shoaling above and below the AAIW, and the AAIW layer is shoaling by about 200 dbar. Additionally, the salinity at the surface and in the AAIW layer is reduced by about 0.1 psu. The shoaling of the isolines (through changes in the layer thickness) and the changes of the water properties in layers (bound by isopycnals) together give rise to changes of the bulk properties. For the comparison, the bulk properties for September 1997 were estimated the same way as those for March 1997, i.e. the ring radius (which did not change significantly according to velocity and hydrographic observations), the reference profile and the integration depths for both months were the same (see Section 3.1).

In the upper 800 m the AHA and the ASA decreased by about 20%, and the APE decreased by about 50% (Table 1). With increasing integration depths the differences between the March and the September estimates increase to about 30% (AHA and ASA) and about 70% (APE) for the integration limit of 1600 m. The reduction of the AHA (ASA) is caused by the deepening and cooling (freshening) of the mixed layer and by the lateral mixing throughout the water column. Below the mixed layer the mixing leads to a shoaling of the isotherms and isohalines (a more detailed discussion of the mixing processes follows in Section 4.3). If the erosion of the water properties in the ring occurred at the same speed at all depths within the upper 1600 m, the percentages of reduction would be the same throughout the water column. Since the reduction of the anomalies increases with increasing integration depth, the importance of mixing also must increase with increasing depth. The reductions for the intermediate depth layers can be derived from the values given in Table 1. In the AAIW layer (800–1100 m) the reductions for AHA and ASA are about 30% and about 40%, respectively. For the layer 1100–1600 m the reductions for AHA and ASA are about 70%.

The changes of the characteristics of ring A are not limited to the hydrography. A comparison of

the results from the March survey with those obtained by Garzoli et al. (1999) from the September survey shows a strong change in the speed–radius relationship. In March 1997 the velocity data outside of a radius of about 80 km were dominated by strong interactions between the surrounding cyclones and ring A (Fig. 6). In contrast to this the September survey clearly revealed the maximum speed and the core radius (50 cm s^{-1} at about 100 km; Garzoli et al., 1999, their Fig. 6). Inside the 80 km radius the speeds near the surface (based on ADCP data) and in the AAIW layer (based on RAFOS data), as observed during the two surveys, are similar. (In the AAIW layer two of the estimates for September are slightly lower, and one is slightly higher than the estimates for March; Table 4). This change of the velocity distribution indicates that ring A reached a more quiescent region in September, where interactions with other eddies are rare.

From here on the focus will be on the AAIW layer into which the RAFOS floats were deployed. The changes of the anomalies of ring A indicate that the Indian Ocean AAIW carried into the Cape Basin by Agulhas Rings is readily mixed with background water (which is primarily water from mesoscale features) in the eastern Cape Basin (in the Cape Cauldron, Boebel et al., 2003a). The vigorous mixing is mirrored in the large variability of the temperature/salinity relationship in this region, and in the transition of the RAFOS floats from ring A to surrounding features and vice versa (this will be discussed in Section 4.3). In the western Cape Basin, Atlantic and Indian Ocean AAIW have merged into an intermediate layer of nearly homogenous composition. Trapping of AAIW nevertheless occurred, as witnessed by RAFOS floats that were carried westward over the Walvis Ridge inside these rings (Richardson and Garzoli, 2003).

4.3. Ring/environment interaction and mixing

Having established the differences between the properties of ring A in March and September 1997, it is natural to ask how these changes came about. For the near-surface thermostad it has already been discussed that wintertime air–sea

interaction led to a cooling and deepening of the mixed layer. However, what are the processes responsible for the observed changes at intermediate depth, i.e. the significant weakening of the ring-environment property contrast? The trajectories together with the hydrographic records from the RAFOS floats and the kinematics of ring A give insight into this subject. In this section, distances from the ring center are based on the positions derived from the steric height fields (Table 2), except for the distances during the float deployment (Table 3).

The anticyclonic looping of all five RAFOS floats deployed into ring A stopped within about 2 months after they were launched (Fig. 7). There are essentially four possible causes for the disappearing of the ring signals from a trajectory: (a) eddy–eddy interactions, (b) changes in the trapping depth and radius of the ring, (c) mixing between the ring and nearly quiescent surrounding water, and (d) disintegration of the ring. Possibility (d) can be excluded since the ring remains visible in the steric height fields, and since the RAFOS floats launched into the ring in September were looping. Possibilities (a)–(c) and their role in the mixing processes in the Cape Basin will be discussed in the light of evidence from the trajectories and the other data sets.

Eddy–eddy interactions can be separated into two phenomena. One is marked by a transition of a RAFOS float from an anticyclone to a cyclone or vice versa. Two processes may explain the fact that floats leave the ring. Strong interaction between an anticyclone and a cyclone generates a high-speed jet between them (essentially the two eddies form a dipole, Flierl, 1981). This high speed is likely to generate turbulences and thus might trigger the subsequent ejection of water parcels (and RAFOS floats) from ring A. The other occurs if two anticyclones are so close together that a RAFOS float can go from one to the other with only an intermittent period of cyclonic drift.

The trapping of a water parcel in an eddy depends on the relationship between the translation speed and the swirl speed (Flierl, 1981). Flierl's basic conclusion is that the water is trapped inside a ring if the swirl speed is greater than the translation speed. Under this scenario,

variations of the translation speed give rise to variations in the trapping depth and radius. The swirl speeds at intermediate depth in ring A were in the range of 14–40 cm s^{-1} (Table 4). Five periods were characterized by a translation speed of 10 cm s^{-1} or more (Table 2). The higher speeds are likely to have an effect on the timing of the departure of a RAFOS float from ring A.

RAFOS 216 and RAFOS 183 (black and red trajectories in Fig. 7) represent examples of interactions of ring A with a cyclone. They were ballasted to drift at different depths and deployed at different distances from the ring center. Initially, RAFOS 183 was 200 m below RAFOS 216 and 20 km farther away from the center of ring A (Table 3). At first, the two RAFOS floats followed parallel pathways including the transition from ring A to a cyclone in the west. The similarities of the early pathways confirm that ring A reaches down to layers below the AAIW and they indicate that the cyclones affect the flow down to similar depths. Their pathways separate as RAFOS 216 entered another anticyclone and RAFOS 183 stayed in the cyclone.

RAFOS 216 accelerated around 10 April (from $18 \pm 4 \text{ cm s}^{-1}$ for 31 March–8 April to $34 \pm 5 \text{ cm s}^{-1}$ for 12–22 April). During this period the distance from the ring center increased from 49 to 86 km. Note that the 49 km is an approximation (no steric height field is available for 8 April). This introduces an error of about 10 km (based on the mean translation speed of the ring between 2 and 12 April given in Table 2). The acceleration phase coincides with the transition to the cyclone. At the time when RAFOS 216 was about to leave ring A the translation speed of the ring was about 10 cm s^{-1} , while the speed of the RAFOS float was nearly twice as large (before the acceleration). This indicates that the RAFOS float is still within the theoretical trapping depth of the ring. Therefore, the interaction of ring A with the cyclone was crucial for the termination of the anticyclonic drift of RAFOS 216. After less than half a revolution RAFOS 216 left the cyclone and drifted around an anticyclone south of ring A before it was re-entrained into ring A shortly after 22 May (Fig. 7).

The hydrographic records of RAFOS 216 reveal only small variations until early April (black in

Fig. 9). After this initial phase, but before 8 April, the pressure and temperature dropped by nearly 50 dbar and 0.5°C , respectively, whereas the salinity remained nearly constant. After about 10 more days of nearly unchanged hydrographic properties another drop in the values of the pressure and the temperature occurred around mid-April (i.e. shortly after the pronounced acceleration of the RAFOS float). The pressure decrease was nearly the same as before but the temperature decrease was twice as large. Simultaneously, the salinity decreased by 0.1 psu, giving rise to the departure from the temperature/salinity relationship encountered during the March survey (Fig. 10e), as the distance between RAFOS 216 and the ring center increases rapidly (to 366 km on 22 April). Assuming that the float was carried out of ring A together with a water parcel it is obvious that this water parcel quickly lost its characteristic hydrographic properties.

The history of RAFOS 183, while similar to that of RAFOS 216, reveals some differences. RAFOS 183 left the ring 14 days before RAFOS 216 (on 3 April, Table 3) and drifted around the western cyclone in a nearly complete loop (red trajectory in Fig. 7). The pressure and temperature recorded by RAFOS 183 (red in Fig. 9) changed only by 25 dbar and 0.3°C shortly after the transition, whereas the salinity did not change significantly, i.e. the temperature/salinity relation stayed close to the relationship observed prior to the deployment of the float (Fig. 10a). The main reason for this is that RAFOS 183 was deployed too far away from the center of ring A to record the temperature/salinity relation of the core (Table 3).

Contrasting the early escape of these two floats, RAFOS 184 and RAFOS 200 remained inside the ring nearly 1 month longer (cyan and green trajectory in Fig. 7). The vertical distance between them was about 200 m, and their initial distance from the ring center differed by about 30 km (Table 3). Their trajectories converged and both followed a nearly parallel track as they experienced a quick transition from ring A to an anticyclone in the west in the first half of May. It is noted that the deeper RAFOS float with a larger initial distance from the center of the ring remains trapped inside of it for about one more week than

the other RAFOS float (Table 3). This is indicative for a very turbulent regime.

The distance between RAFOS 184 and the ring center increased from 24 to 59 km on 2 April and then decreased again to 21 km on 12 April. The latter may not have been the closest position, since the highest temperature, pressure, and salinity were recorded 4 days earlier (8.9°C , 836 dbar, 34.7 psu, cyan in Fig. 9). Fig. 3 shows that similar values occurred near the strongest depression of the 10°C isotherm. Until mid-April the hydrographic properties decreased gradually, followed by a more rapid decrease until 27 April (which corresponds to the jump from the saltier to the fresher temperature/salinity curve, Fig. 10b). During this period the distance between RAFOS 184 and the ring center increases to 55 km on 22 April and 132 km on 2 May, as the RAFOS float accelerated from 9 cm s^{-1} (northward, 2–12 April) to 15 cm s^{-1} (northward, 12–22 April) and finally to 28 cm s^{-1} (westward, 22 April–2 May). The float probably left the ring on or shortly after 22 April and was entrained into the anticyclone west of ring A around 2 May. The latter caused an initial increase of the hydrographic properties until 5 May, followed by a decrease until a plateau is reached around mid-June (the float stayed in the anticyclone until the beginning of July, i.e. this decrease is not due to a detrainment of the float).

For RAFOS 200 the transition to the western anticyclone (taking place between 27 April and 15 May) does not cause any permanent large changes in the hydrographic record (green in Fig. 9). A probably short-lived (note the long gaps during this period) significant decrease of the temperature and the pressure is apparent in the time series, but this does not significantly affect the salinity. Later on, in the second half of May the pressure and the temperature have nearly reached the level they had before 27 April. The weak signals in this record can be attributed to three facts. First, from the temperature/salinity diagram (Fig. 10c) it becomes apparent that, in the temperature range in question (more than 8°C), the temperature/salinity relationship of the two profiles (obtained south of ring A and at the launch position) is nearly the same. Therefore, a salinity change cannot be interpreted as a transition from one water body

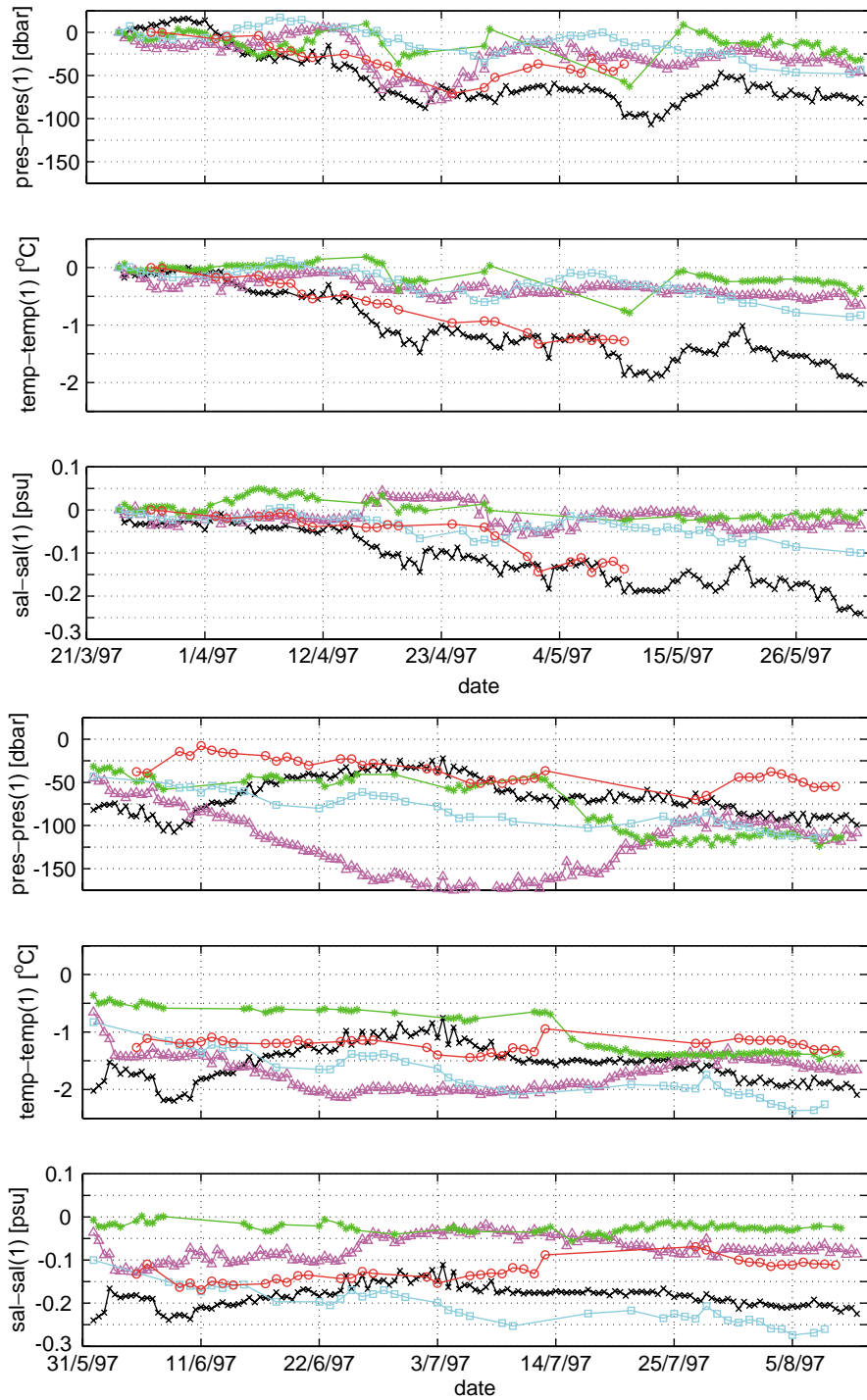


Fig. 9. Deviation of pressure (top), temperature (middle) and salinity (bottom) from first observed values for RAFOS 183 (red circles), RAFOS 184 (cyan squares), RAFOS 200 (green asterisks), RAFOS 215 (magenta triangles) and RAFOS 216 (black crosses).

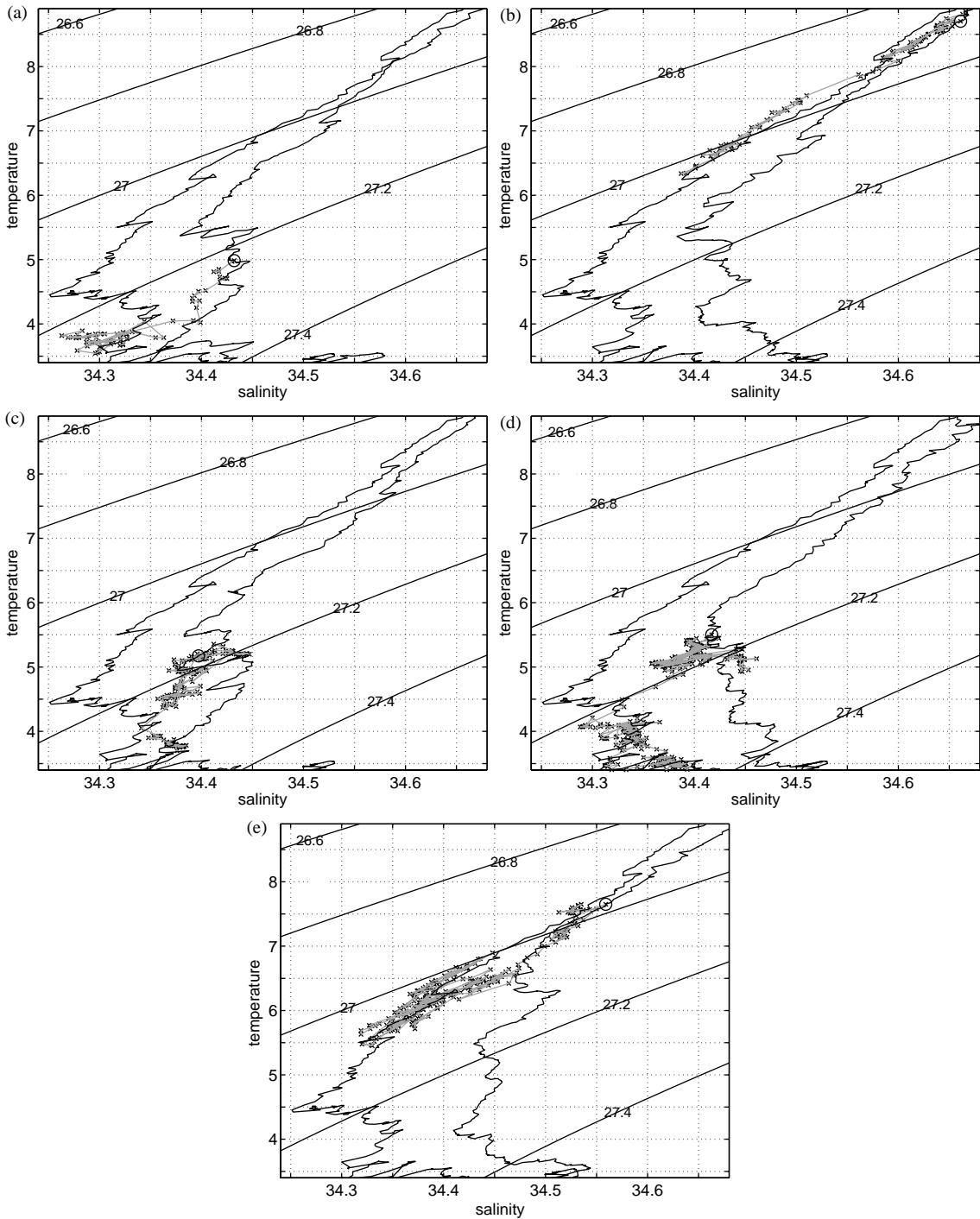


Fig. 10. Temperature/salinity diagrams with lines of equal density (σ_0) from two CTD stations (lines) and RAFOS floats (crosses). One station was taken at the launch position of each RAFOS float. The other station was just south of ring A (near 38°S, 16°E, marked with an asterisk in Fig. 2). The first measurement by a RAFOS float has been marked with a circle. (a) RAFOS 183, (b) RAFOS 184, (c) RAFOS 200, (d) RAFOS 215, and (e) RAFOS 216.

to another. Second, RAFOS 200 was too far from the ring center (Table 3) to record the core properties of ring A. Third, during the second half of May RAFOS 200 stayed inside of the western anticyclonic, which is likely to have similar water characteristics as ring A.

Another case is RAFOS 215, which was deployed at a distance of 39 km from the ring center to drift at 1024 dbar (Table 3). It stayed in ring A for two full revolutions before it was captured by a cyclone to the north of the ring (magenta in Fig. 7). This RAFOS float is the only one where the translation speed exceeds the swirl speed (by at least 5 cm s^{-1} , Tables 2 and 4). In accordance with Flierl (1981) this indicates that the drop-out can be attributed to a (temporary) change of the trapping depth of ring A. The temperature and salinity decrease during the transition around the beginning of June 1997 (magenta in Fig. 9) was much sharper than for the other RAFOS floats. The temperature/salinity diagram shows a quick transition of RAFOS 215 from the relatively salty water in the ring to the less salty surrounding water (Fig. 10d).

The given examples show that a vigorous exchange of water between the ring and its surroundings occurred at intermediate depth. The exchanges at different depths are likely to occur at different times (and for different reasons). This causes the interleaving of water parcels with different hydrographic properties (which can be seen in Fig. 10) and therefore leads to enhanced mixing. The highest variability in the upper 1600 m was found in the AAIW layer, where the density often changed only slightly with depth due to the counter-effects of the vertical temperature and salinity gradients on the density. Thus mixing can be induced by double diffusion as well as turbulence. The density ratio $R_\rho = \alpha\Delta T/(\beta\Delta S)$ is a measure for the likeliness of the double diffusive process (Schmitt, 1981). Here $\alpha = -\rho^{-1}\delta\rho/\delta T$ is the thermal expansion coefficient, and $\beta = \rho^{-1}\delta\rho/\delta S$ is the haline contraction coefficient. ρ , T and S are density, temperature, and salinity, respectively. Small density ratios are favorable for double diffusion and thus allow the growth of salt fingers. According to Schmitt (1981) salt fingers are of minor importance for density

ratios of two or more. When R_ρ approaches one, salt finger development will be strong. Negative density ratios indicate favorable conditions for vertical instability.

Fig. 11 shows that the density ratio in ring A mostly exceeded two between 200 and 900 dbar. In the AAIW layer, which extends from 900 to 1400 dbar in the ring center, the density ratio decreases with increasing depth. At first glance this decrease seems quite rapid around 900 dbar, but this is primarily due to one of the small-scale features superimposed on a more gradual decrease between 800 and 1200 dbar. Within 800–1000 dbar (this range corresponds roughly to the upper part of the AAIW layer) the density ratio is mostly between one and two. In the next 200 m thick layer the density ratio varies between zero and one, and below 1200 dbar the density ratio was within -0.5 and 0.5 . Outside ring A between 500 and 1500 dbar (i.e. throughout and below the AAIW layer) the density ratio was mostly smaller than one and negative values are found frequently. These results suggest that double diffusion is likely to play an important role for the mixing in the upper AAIW layer inside the ring. In the lower AAIW layer in the ring, and in the whole AAIW

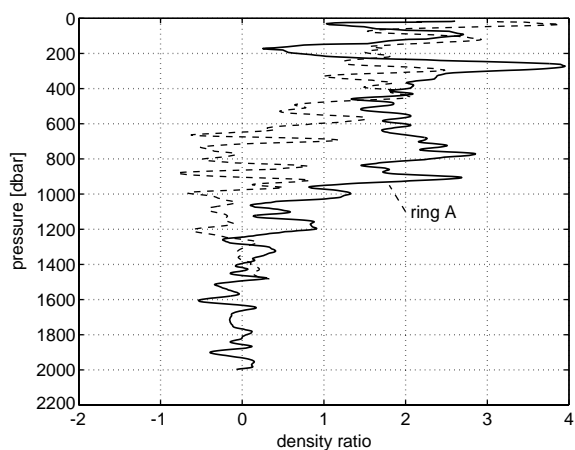


Fig. 11. Profiles of mean density ratio (R_ρ). The solid line is derived from five density ratio profiles in ring A, the dashed line is derived from five profiles north of ring A. All profiles are from the March survey. Their locations are along the cruise track extending from Cape Town towards southwest to south (Fig. 2).

layer outside of the ring vertical instability becomes important.

The relative importance of turbulent and double diffusive processes for along-track changes cannot be quantified from the available data set, but it seems likely that turbulent processes enhance the erosion of properties within a water parcel surrounding a float. Both processes together are responsible for the quick changes of the temperature/salinity relationship derived for RAFOS floats each time a transition from an anticyclone to a cyclone occurred (RAFOS 183, 215 and 216). This is mirrored in the high variability of the temperature/salinity relationship around the salinity minimum of the AAIW inside and in the vicinity of ring A (Fig. 10). Transitions from one anticyclone to the next are usually accompanied by nearly stable temperature/salinity relationships if the two anticyclones are as close together as observed around the end of April (less than 300 km apart, RAFOS 184 and 200).

5. Summary

This study describes and analyzes the origin, the translation and the changes of Agulhas Ring A that was visited during two research cruises in March and September 1997. The data set obtained during the cruises is complemented with Lagrangian velocity measurements at intermediate depth and steric height fields derived from satellite observations.

Ring A was formed in the austral summer of 1996/1997. Most likely it detached from the Agulhas Retroflection in December 1996 near 38°S, 18°E. This conclusion is supported by the absence of thermostad layers (like the South Indian Subtropical Mode Water, Olson et al., 1992; or deep well-mixed convective layers, Mey et al., 1990); some of these layers originate in the southwestern part of the Agulhas Retroflection region. Between 22 and 24 March ring A was observed in situ near 37°S, 16°E (about 200 km west of its formation region). In the following 5 months ring A crossed two-thirds of the Cape Basin (about 930 km, Figs. 5 and 7).

RAFOS floats were deployed in March 1997 to track ring A. They were detrained after two revolutions or less (Fig. 7). Some RAFOS floats entered cyclones and others were entrained into other anticyclones after brief periods of cyclonic drift. Re-entrainments of RAFOS floats into ring A also were observed. These observations and the satellite images (Fig. 5) show that ring A interacted strongly with the surrounding water in a regime that consisted of numerous anticyclones and cyclones. The frequent transition of RAFOS floats from ring A to surrounding features or vice versa indicates that water exchanges occurred often. The vigorous interaction was an important underlying cause for the high variability of the temperature/salinity relationship inside and outside of the ring, and it gave rise to a considerable change of the hydrographic properties of ring A during the 5 months between the two surveys (Table 1). The ring's available heat and salt anomalies decrease by 20–30% during the 5 months. The given range depends on the integration depth. A significant part of these changes can be attributed to the Antarctic Intermediate Water layer.

A large difference exists between the eastern and the western Cape Basin. The western Cape Basin is characterized by a weaker variability with less ring–environment interactions in the Antarctic Intermediate Water layer. This is mirrored in the difference between trajectory characteristics of the March and the September 1997 RAFOS float deployments (Fig. 7). The former left the ring after a short time whereas two of the latter stayed inside ring A until it crossed over the Walvis Ridge.

It is important to quantify the influence of the inter-oceanic exchange of waters south of Africa on the South Atlantic as a whole. To do this adequately, heat loss to the atmosphere from Agulhas Rings needs to be determined to establish how much they retain that can eventually be carried into the wider Atlantic (Arhan et al., 1999). This is, however, not the only way in which rings relinquish their anomalous load of heat and salt. There are strong indications that Agulhas rings already lose most of their energy in the Cape Basin (e.g., Schouten et al.,

2000). The results presented here, and elsewhere in this volume (Boebel et al., 2003a; Lutjeharms et al., 2003), give indications how this may happen. It is shown that mixing of intermediate waters in Agulhas Rings as well as exchanges with ambient waters are vigorous and complex processes, leading to the rapid dissipation of Agulhas Rings well before they reach the Walvis Ridge. These results thus lay a good foundation for subsequent research programmes such as mixing in Agulhas Rings experiment (MARE; Lutjeharms et al., 2000; van Aken et al., 2003) aimed specifically at a study of these processes.

Acknowledgements

This research was carried out in part under the auspices of the Cooperative Institute for Marine and Atmospheric Studies (CIMAS), a joint institute of the University of Miami and the National Oceanic and Atmospheric Administration (NOAA), cooperative agreement #NA67RJ0149. The Naval Research Laboratory received support for the work on the Modular Ocean Data Assimilation System from the Oceanographer of the Navy via the Space and Naval Warfare Systems Command PMW155 under PE 0603207N. The German contribution was supported by the Bundesministerium für Bildung, Wissenschaft, Forschung und Technologie (BMBF/FZ 03F0121A) and the Humboldt Stiftung. The South African contribution was financially supported by the National Research Foundation of South Africa and the University of Cape Town. The Woods Hole Oceanographic Institution received funding from the National Science Foundation (NSF grant #OCE95-28574). We want to thank the reviewers for their valuable comments.

References

- Arhan, M., Mercier, H., Lutjeharms, J.R.E., 1999. The disparate evolution of three Agulhas rings in the South Atlantic Ocean. *Journal of Geophysical Research* 104 (C9), 20,987–21,005.
- Beismann, J.O., Käse, R.H., Lutjeharms, J.R.E., 1999. On the influence of submarine ridges on translation and stability of Agulhas rings. *Journal of Geophysical Research* 104, 7897–7906.
- Boebel, O., Barron, C., 2003. A comparison of in-situ float velocities with altimeter derived geostrophic velocities. *Deep-Sea Research II*, this issue (PII S0967-0645(02)00381-8).
- Boebel, O., Schultz Tokos, K.L., Zenk, W., 1995. Calculation of salinity from neutrally buoyant RAFOS floats. *Journal of Atmospheric and Oceanic Technology* 12 (4), 923–934.
- Boebel, O., Schmid, C., Jochum, M., 1997. Deployment of RAFOS floats in the Cape Basin. *International WOCE Newsletter* 28, 30–33.
- Boebel, O., Schmid, C., Jochum, M., 1998a. Cruise Report of the *Polarstern ANT XIV/4* cruise: Physical Oceanography. *Berichte zur Polarforschung (Reports on Polar Research)* no. 259, 1998, pp. 6–20. In: Fütterer, D.K., Riemann, D.F. (Eds.), *Die Expedition ANTARKTIS-XIV/4 mit FS "Polarstern" 1997; The Expedition ANTARKTIS-XIV/4 of RV "Polarstern" in 1997*.
- Boebel, O., Duncombe Rae, C., Garzoli, S., Lutjeharms, J., Richardson, P., Rossby, T., Schmid, C., Zenk, W., 1998b. Float experiment studies interocean exchanges at the tip of Africa. *EOS, Transactions, American Geophysical Union* 79 (1), 1,7–8.
- Boebel, O., Lutjeharms, J.R.E., Rossby, T., Zenk, W., 2003a. The Cape Cauldron: A regime of turbulent interocean exchange. *Deep-Sea Research II*, this issue (PII S0967-0645(02)00379-X).
- Boebel, O., Rossby, T., Lutjeharms, J.R.E., Zenk, W., Barron, C., 2003b. Path and variability of the Agulhas Return Current. *Deep-Sea Research II*, this issue (PII S0967-0645(02)00377-6).
- Byrne, D.A., Gordon, A.L., Haxby, W.F., 1995. Agulhas eddies: a synoptic view using GEOSTAT ERM data. *Journal of Physical Oceanography* 25 (5), 902–917.
- Carnes, M.C., Fox, D., Rhodes, R., 1996. Data assimilation in a North Pacific Ocean monitoring and prediction system. In: Malnotte-Rizzoli, P. (Ed.), *Modern Approaches to Data Assimilation in Ocean Modelling*. Elsevier, New York, pp. 319–345.
- Clement, A.C., Gordon, A.L., 1995. The absolute velocity field of Agulhas eddies and the Benguela Current. *Journal of Geophysical Research* 100 (C11), 22,591–22,601.
- de Ruijter, W.P.M., Biastoch, A., Drijfhout, S., Lutjeharms, J.R.E., Matano, R.P., Pichevin, T., van Leeuwen, P.J., Weijer, W., 1999. Indian–Atlantic inter-ocean exchange: dynamics, estimation and impact. *Journal of Geophysical Research* 104 (C9), 20,885–20,911.
- Duncombe Rae, C.M., 1991. Agulhas Retroreflection Rings in the South Atlantic Ocean: an overview. *South African Journal of Marine Science* 11, 327–344.
- Duncombe Rae, C.M., Garzoli, S.L., Gordon, A.L., 1996. The eddy field of the southeast Atlantic Ocean: a statistical census from the Benguela Sources and Transports Project. *Journal of Geophysical Research* 101 (C5), 11,949–11,964.

- Flierl, G.R., 1981. Particle motions in large-amplitude wave fields. *Geophysical and Astrophysical Fluid Dynamics* 18, 39–74.
- Fox, D.N., Teague, W.J., Barron, C.N., Carnes, M.R., Lee, C.M., 2002. The modular ocean data assimilation system (MODAS). *Journal of Atmospheric and Oceanic Technology* 19 (2), 240–252.
- Garzoli, S.L., Gordon, A.L., Kamenkovich, V., Pillsbury, D., Duncombe Rae, C., 1996. Variability and sources of the southeastern Atlantic circulation. *Journal of Marine Research* 54, 1039–1071.
- Garzoli, S.L., Richardson, P.L., Duncombe Rae, C.M., Fratantoni, D.M., Goñi, G., Roubicek, A.J., 1999. Three Agulhas rings observed during the Benguela Current Experiment. *Journal of Geophysical Research* 104 (C9), 20,971–20,985.
- Goñi, G., Garzoli, S.L., Roubicek, A.J., Olson, D.B., Brown, O.B., 1997. Agulhas ring dynamics from TOPEX/POSEIDON satellite altimeter data. *Journal of Marine Research* 55, 861–883.
- Gordon, A.L., 1985. Indian–Atlantic transfer of thermocline water at the Agulhas retroflection. *Science* 227, 1030–1033.
- Gordon, A.L., 1986. Inter-ocean exchange of thermocline water. *Journal of Geophysical Research* 91 (C4), 5037–5046.
- Gordon, A.L., Lutjeharms, J.R.E., Gründlingh, M.L., 1987. Stratification and circulation at the Agulhas Retroflection. *Deep-Sea Research* 34A (4), 565–599.
- Jacobs, G.A., Barron, C.N., Rhodes, R.C., 2001. Mesoscale characteristics. *Journal of Geophysical Research* 106 (C9), 19581–19595.
- Kamenkovich, V.M., Leonov, Y.P., Nechaev, D.A., Byrne, D.A., Gordon, A.L., 1996. On the influence of bottom topography on the Agulhas eddy. *Journal of Physical Oceanography* 26, 892–912.
- Lutjeharms, J.R.E., 1996. The exchange of water between the South Indian Ocean and the South Atlantic. In: Wefer, G., Berger, W.H., Siedler, G., Webb, D.J. (Eds.), *The South Atlantic: Present and Past Circulation*. Springer, Berlin, Heidelberg, pp. 121–124.
- Lutjeharms, J.R.E., Cooper, J., 1996. Interbasin leakage through Agulhas Current filaments. *Deep-Sea Research I* 43, 213–238.
- Lutjeharms, J.R.E., Gordon, A.L., 1987. Shedding of an Agulhas Ring observed at sea. *Nature* 325, 138–140.
- Lutjeharms, J.R.E., van Ballegooyen, R.C., 1988. The retroflection of the Agulhas Current. *Journal of Physical Oceanography* 18 (11), 1570–1583.
- Lutjeharms, J.R.E., Boebel, O., Rossby, T., 1997. KAPEX: an international experiment to study deep water movement around southern Africa. *South African Journal of Science* 93 (9), 377–388.
- Lutjeharms, J.R.E., de Ruijter, W.P.M., Ridderinkhof, H., van Aken, H., Veth, C., van Leeuwen, P.J., Drijfhout, S., Jansen, J.H.F., Brummer, G.-J.A., 2000. MARE and ACSEX: new research programmes on the Agulhas Current system. *South African Journal of Science* 96, 105–110.
- Lutjeharms, J.R.E., Boebel, O., Rossby, T., 2003. Agulhas cyclones. *Deep-Sea Research II*, this issue (PII S0967-0645(02)00378-8).
- McDonagh, E.L., Heywood, K.J., Meredith, M.P., 1999. On the structure, paths and fluxes associated with Agulhas Rings. *Journal of Geophysical Research* 104 (C9), 21,007–21,020.
- Mey, R.D., Walker, N.D., Jury, M.R., 1990. Surface heat fluxes and marine boundary layer modification in the Agulhas retroflection region. *Journal of Geophysical Research* 95 (C9), 15,997–16,015.
- Müller, T.J., Holfort, J., Delahoyde, F., Williams, R., 1995. MKIIIIB CTD: improving its system output. *Deep-Sea Research I* 42 (11/12), 2113–2126.
- Olson, D.B., Evans, R.H., 1986. Rings of the Agulhas current. *Deep-Sea Research* 33A (1), 27–42.
- Olson, D.B., Fine, R.A., Gordon, A., 1992. Convective modifications of water masses in the Agulhas. *Deep-Sea Research A* 39 (Suppl. 1), S163–S181.
- Reid, J.L., 1989. On the total geostrophic circulation of the South Atlantic Ocean: flow patterns, tracers and transports. *Progress in Oceanography* 23, 149–244.
- Richardson, P.L., Garzoli, S.L., 2003. Characteristics of Intermediate Water flow in the Benguela Current as measured with RAFOS floats. *Deep-Sea Research II*, this issue (PII S0967-0645(02)00380-6).
- Rossby, T., Dorson, D., Fontane, J., 1986. The RAFOS system. *Journal of Atmospheric and Oceanic Technology* 3 (9), 672–679.
- Schmitt, R.W., 1981. Form of the temperature–salinity relationship in the Central Water: evidence for double-diffusive mixing. *Journal of Physical Oceanography* 11 (7), 1015–1026.
- Schouten, M.W., de Ruijter, W.P.M., van Leeuwen, P.J., Lutjeharms, J.R.E., 2000. Translation, decay and splitting of Agulhas rings in the southeastern Atlantic ocean. *Journal of Geophysical Research* 105 (C9), 21,913–21,925.
- Shannon, L.V., Hunter, D., 1988. Notes on Antarctic intermediate water around Southern Africa. *South African Journal of Marine Science* 6, 107–117.
- Shannon, L.V., Nelson, G., 1996. The Benguela: large scale features and processes and system variability. In: Wefer, G., Berger, W.H., Siedler, G., Webb, D.J. (Eds.), *The South Atlantic: Present and Past Circulation*. Springer, Berlin, Heidelberg, pp. 163–210.
- Valentine, H.R., Lutjeharms, J.R.E., Brundrit, G.B., 1993. The water masses and volumetry of the southern Agulhas Current region. *Deep-Sea Research I* 40 (6), 1285–1305.
- van Aken, H., van Veldhoven, A., Veth, C., de Ruijter, W.P.M., van Leeuwen, P.J., Drijfhout, S., Whittle, C., Rouault, M., 2003. Observations of a young Agulhas ring, Astrid, during MARE, the Mixing of Agulhas Rings Experiment. *Deep-Sea Research II*, this issue (PII S0967-0645(02)00383-1).

- van Ballegooyen, R.C., Gründlingh, M.L., Lutjeharms, J.R.E., 1994. Eddy fluxes of heat and salt from the southwest Indian Ocean into the southeast Atlantic Ocean: a case study. *Journal of Geophysical Research* 99 (C7), 14,053–14,070.
- Weijer, W., de Ruijter, W.P.M., Dijkstra, H.A., van Leeuwen, P.J., 1999. Impact of interbasin exchange on the Atlantic overturning circulation. *Journal of Physical Oceanography* 29 (9), 2266–2284.